

VERIFICATION OF A BINARY FLUID SOLIDIFICATION MODEL USING SEMI-ANALYTICAL SOLUTION OF 1D HEAT DIFFUSION EQUATION

Tomasz Waławczyk*,¹, Michael Schäfer

Institute of Numerical Methods in Mechanical Engineering, Technische Universität Darmstadt,
Dolivostr. 15, Germany

¹ Present address: Institute of Aeronautics and Applied Mechanics, Warsaw University of Technology,
Warszawa, ul. Nowowiejska 24, Poland

The aim of the present work is to verify a numerical implementation of a binary fluid, heat conduction dominated solidification model with a novel semi-analytical solution to the heat diffusion equation. The semi-analytical solution put forward by Chakaraborty and Dutta (2002) is extended by taking into account variable in the mushy region solid/liquid mixture heat conduction coefficient. Subsequently, the range in which the extended semi-analytical solution can be used to verify numerical solutions is investigated and determined. It has been found that linearization introduced to analytically integrate the heat diffusion equation impairs its ability to predict solidus and liquidus line positions whenever the magnitude of latent heat of fusion exceeds a certain value.

Keywords: heat diffusion, semi-analytical solution, numerical methods, binary fluid solidification

1. INTRODUCTION

The main difficulty in numerical simulations of casting of metal alloys (e.g. Al-4.1%Cu, Sn-10%Pb) is the broad range of length and time scales that must be reconstructed. In order to avoid direct simulation of crystal growth, in engineering applications, problems in the modeling of the smallest length scales are resolved by the introduction of a volume averaging or mixture assumption. The volume averaging of flow and heat transfer governing equations give rise to the Darcy–Brinkman model for interstitial fluids (Bars and Worster, 2006), whereas the mixture theory allows equations for solid-liquid systems to be derived (Bennon and Incropera, 1987; Kurz and Fischer, 1980; Worster, 1986). In both approaches, the phase change diagram and the macrosegregation model supply the physics of the phase transition and growth of the mushy zone at the microstructure level, where the smallest length scale is determined by details of the dendrite geometry.

After the volume averaging is performed, the smallest time scales which have to be resolved in numerical simulations are related to the flow phenomena in bulk fluid and porous (mushy zone) regions. Their accurate reconstruction is crucial for the prediction of a macrosegregation pattern, i.e. nonuniform concentration of a solute. Since macrosegregation can lead to a variety of casting defects impairing the final quality of the product, its determination, monitoring and minimization is of primary interest to casting

* Corresponding author, e-mail: twacl@fmb.tu-darmstadt.de, twacl@meil.pw.edu.pl <http://journals.pan.pl/dlibra/journal/98834>

engineers. At the other end, the largest time scales of the solidification process are in the order of hours or days. They are inherited from a need to model heat conduction during cooling of cast parts, e.g. a ship engine block. Because alloys have low thermal diffusivity and because macrosegregation needs to be predicted simultaneously, simulations of the casting and solidification processes in industrial configurations are computationally demanding and time-consuming.

A multiscale approach, introduced by averaging of the governing equations and by modeling the sub-grid processes, allows for a reliable approximation of the exact solidification model. However, a solution of averaged equations requires monitoring of the numerical procedure. This involves making certain the mesh resolution and grid node distribution are appropriate, as well as a properly selecting the solver parameters, in particular, ensuring an accurate solution of the energy conservation equation directly coupled with a solidification model.

To verify the numerical solutions of these averaged equations their semi-analytical solutions, derived with additional physical constraints, are often used. The semi-analytical solutions to the problem of unidirectional solidification of binary fluids were investigated by Braga and Viscanta (1990), Chakaraborty and Dutta (2002) and Voller (1997). In this latter work a comprehensive overview of the semi-analytical solutions for the unidirectional solidification of binary fluids can be found. In spite of their inherent drawbacks, Voller (1997) concludes the semi-analytical solutions can be considered as a useful tool for verification of numerical codes. The common feature of aforementioned semi-analytical solutions is the transformation of the partial differential energy conservation equation into a set of ordinary differential equations using the similarity variable $\eta = xg(t)$, where $g(t) = 1/(2\sqrt{\alpha_s t})$. Since the resulting differential equations in the solid and liquid phase are linear, they are solved analytically therein. Obtained temperature profiles are used to specify heat fluxes at the solid and liquid sides of both solidification fronts, respectively; these fluxes are dependent on the non-dimensional positions of solidus η_S and liquidus fronts η_L . The main difference between aforementioned works, lies in the approach to the solution of the heat diffusion equation in the mushy zone. For example, Braga and Viscanta (1990) search only for the position of η_L . In their work, data from the experiment are used to set the boundary conditions for temperature at the cold wall kept above eutectic temperature. Having found the analytical solution of the heat diffusion equation in the liquid, the heat flux from the liquid side is used in the convergence criterion, i.e., the boundary condition for heat flux at liquidus line. The η_L is obtained through corrections in the iterative procedure, once the equality between fluxes on both sides of the liquidus front is achieved, η_L is determined. We note, in the work of Braga and Viscanta (1990) both c_M and k_M are variable inside the mushy zone giving rise to the new non-linear terms in the heat diffusion equation.

Voller (1997) uses another approach, in this work it was assumed that $c_M = c_S = c_L$ and $k_M = k_S = k_L$ are constant in the whole domain including the mushy zone. However, $\rho_S \neq \rho_L$ which results in a model allowing to take into account the velocity field generated by the shrinkage and thus predict macrosegregation due to different volumes of solidified species of binary mixture. Similar to Braga and Viscanta (1990), Voller (1997) also solves the heat diffusion equation numerically, avoiding linearization required to obtain η_S , η_L .

In the present work, we extend the semi-analytical solution to the binary fluid solidification problem put forward by Chakaraborty and Dutta (2002). Instead of the complex numerical procedure, linearization to the heat diffusion equation in the mushy zone is introduced such that an analytical solution to the heat diffusion equation is possible. Subsequently, the derived semi-analytical solution is used to verify a numerical implementation of the binary fluid solidification model, where the phase-change process is driven by heat diffusion.

2. PHYSICAL AND MATHEMATICAL MODELS

The binary fluid solidification model is based on the experimentally determined phase change diagram shown in Fig. 1. It describes the coexistence of a liquid, a solid and a mushy zone developed as a result of a flat solidification front instability caused by constitutional supercooling (Worster, 1986). In the mushy zone, a species *B* with larger concentration solidifies, whereas the solute species *C* is rejected to the liquid solution. The solute *C* rejection increases its local concentration in the binary liquid and decreases the local solidification temperature (see the shaded region depicted in Fig. 1). Such local variations in solidification temperature lead to a solidification front instability and growth of dendrite forest, i.e. the mushy zone.

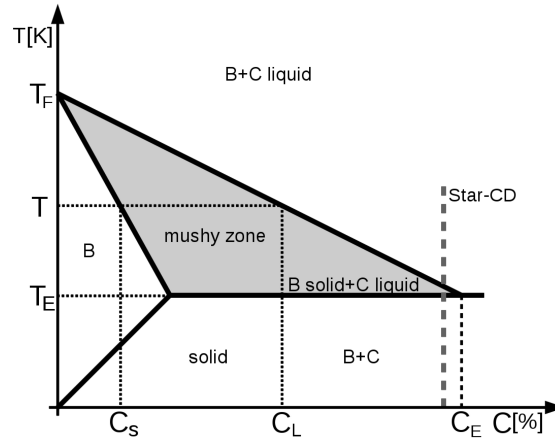


Fig. 1. A binary fluid phase change diagram, shaded region tags conditions (temperature and solute species *C* concentration) for the mushy zone creation. The dashed, vertical line depicts schematically the default solidification model in the Star-CD flow solver $C = \text{const}$

The borders of phase change regions are defined in terms of the solidus and liquidus lines given by $T_{sol} = \max(T_F + m_L C_M / k_P, T_E)$ and $T_{liq} = T_F + m_L C_M$ as functions of the mixture solute concentration $C_M = C_L f_L + C_S f_S$ and thus the local temperature T . The solid mass fraction $f_S = 1 - f_L$ can be determined from the lever rule

$$f_S = \frac{C_M - C_L}{C_S - C_L} = \frac{1}{1 - k_P} \frac{T - T_{liq}}{T - T_F} \quad (1)$$

or from the Scheil model

$$f_S = \left(\frac{C_M}{C_L} \right)^{\frac{1}{1-k_P}} = 1 - \left[k_P \frac{T_{sol} - T_F}{T_F - T} \right]^{\frac{1}{1-k_P}} \quad (2)$$

where it was assumed that $C_S = k_P C_L$ (Bennon and Incropera, 1987; Kurz and Fischer, 1980; Worster, 1986). For brevity, in the present paper we use the lever rule given by Eq. (1). However, all derivations and results presented here can be also obtained for the Scheil model. The coupling of the thermodynamic relations with a flow field is carried out using the mixture model introduced by Bennon and Incropera (1987) and Wang and Beckermann (1993). The mixture model assumes that the solid and liquid phases are uniformly distributed inside the representative control volume with the size large enough to set properties of the medium inside effectively constant. The latter constraint or direct volume averaging of the phases allows to define the mass $f_k = m_k / m$ and the volume $g_k = V_k / V$ fractions, where $k = L, S$; in the present work, we set $\rho_S = \rho_L$ and thus $g_k = f_k$. Hence, the thermophysical properties of the solid/liquid mixture are approximated with the arithmetic mean $\varphi = \varphi_S g_S + \varphi_L g_L$, where φ represents any of the mixture material properties (density, specific heat, etc.) or mixture independent variables (velocity, enthalpy) in the conservation equations. The dynamic viscosity μ_L of the interstitial fluid in the mushy zone and the liquid

alloy is assumed to be constant. Furthermore, the velocity of the solid $u_{i,s} = 0$ and therefore interaction between solid and interstitial fluid is restricted to the mushy zone. Here, Darcy's law with the Karman-Kozeny equation is used for modeling the pressure drop in the porous mushy region, see the last term on the right hand side of Eq. (4). When taking into account the aforementioned simplifications, the continuity and the momentum equations become

$$\frac{\partial u_i}{\partial x_i} = 0 \quad (3)$$

$$\begin{aligned} \frac{\partial \rho u_i}{\partial t} + \frac{\partial \rho u_i u_j}{\partial x_j} = \frac{\partial}{\partial x_j} \left[\mu_L \left(\frac{\partial u_i}{\partial x_j} + \frac{\partial u_j}{\partial x_i} \right) \right] - \frac{\partial p}{\partial x_i} - \frac{\mu_L}{K} u_i - \frac{\partial}{\partial x_j} [\rho (g_L u_{i,L} u_{j,L} - u_i u_j)] + \\ + \rho [1 - \chi(T - T_l) - \psi(C_L - C_l)] g_i \end{aligned} \quad (4)$$

where u_j is the mixture velocity, χ and ψ are thermal and solutal expansion coefficients, and the permeability K is defined by the Karman-Kozeny equation $K = K_0 g_L^3 / (1 - g_L)^2$, where $K_0 = \lambda^2 / 180$ is a material constant determined by the secondary dendrite arm spacing λ .

The energy conservation equation governing heat transport during the solidification process can be written in terms of the mixture enthalpy

$$\frac{\partial \rho h}{\partial t} + \frac{\partial \rho u_j h}{\partial x_j} = \frac{\partial}{\partial x_j} \left(k \frac{\partial T}{\partial x_j} \right) - \frac{\partial}{\partial x_j} [\rho u_j (h_L - h)] \quad (5)$$

defined by the arithmetic mean of the solid h_S and liquid h_L enthalpies $h = h_L g_L + h_S g_S$ where:

$$h_S = c_S T \quad \text{and} \quad h_L = c_L T + L_m \quad (6)$$

Finally, to reconstruct evolution of the solute concentration in the mixture velocity field u_i its transport equation is introduced. After neglecting molecular diffusion of species in the liquid and solid phases, i.e., setting $D_S = D_L = 0$, the solute transport equation reads

$$\frac{\partial \rho C}{\partial t} + \frac{\partial \rho u_j C}{\partial x_j} = - \frac{\partial}{\partial x_j} [\rho u_j (C_L - C)] \quad (7)$$

A complete description and formal derivation of the binary fluid solidification model based on the mixture theory can be found in the works of Bennon and Incropera (1987), Voller and Brent (1989), Wang and Beckermann (1993), whereas comprehensive derivation of the Darcy-Brinkman model is presented by Bars and Worster (2006). For further physical models and their numerical implementations taking into account columnar dendrites and moving equiaxed grains refer for instance to Banaszek and Sreedyński (2013), Sreedyński and Banaszek (2014).

The model described above was implemented in a finite volume flow solver Star-CD with the aid of additional subroutines for extension of the standard user interface supplied by the code developer. Since in Star-CD both the mixture enthalpy h and the temperature T are used in the energy Eq. (5) a procedure allowing recalculation of the local temperature T from the given enthalpy h_g (which is the solution of Eq. (5) at the current time step and outer iteration) is required and is essential for the simulation process. Authors of the present paper implemented a technique using a bi-section method to solve the non-linear equation $h(T, g_s(T)) = h_g$ in each control volume to determine the local temperature T required in Eqs. (1) or (2). The second contribution, was a proper solution of the solute transport equation (Eq. (7)) in the framework of Star-CD (Jakumeit et al., 2012; Waclawczyk and Schäfer, 2016; Waclawczyk et al., 2011). In the present work, only 1D numerical and semi-analytical solutions of the energy conservation equation are studied, respectively, see Eq. (5) and Eq. (11). Therefore herein, we only address the issue of coupling of the binary-fluid solidification model with the energy conservation equation.

3. SEMI-ANALYTICAL SOLUTION IN A SEMI-INFINITE DOMAIN

To verify the energy equation solver coupled with the binary fluid solidification model, we consider a semi-analytical solution of an one-dimensional heat diffusion dominated solidification in a semi-infinite domain. In what follows, we revisit the semi-analytical solution introduced by Chakaraborty and Dutta (2002), and next, its modification is introduced. The extended semi-analytical solution allows to take into account a variation of the thermal conductivity $k_M \neq k_S \neq k_L$ coefficient in the mushy zone.

Let us consider 1D solidification in the semi infinite domain $(0, \infty)$. We assume additionally $\rho = \text{const}$, $u_i = 0$, $c = \text{const}$, $\partial k / \partial x \neq 0$. As enthalpies in solid h_S and liquid h_L are defined by Eqs. (6), the mixture enthalpy reads

$$h = cT + (1 - g_S)L_{ht} \quad (8)$$

Using the above assumptions and substituting Eq. (8) into Eq. (5) the energy equation in the form

$$\rho c \frac{\partial T}{\partial t} - \rho L_{ht} \frac{\partial g_S}{\partial t} = \frac{\partial}{\partial x} \left(k \frac{\partial T}{\partial x} \right) \quad (9)$$

is obtained. Next, it is rewritten using dependence of the solid fraction g_S on temperature

$$\frac{\partial g_S}{\partial t} = \frac{dg_S}{dT} \frac{\partial T}{\partial t} \quad (10)$$

Hence, the problem of heat diffusion during solidification of a binary fluid is described by the parabolic partial differential equation

$$\left(\frac{1}{\alpha_M} - \frac{\rho L_{ht}}{k_M} \frac{dg_S}{dT} \right) \frac{\partial T}{\partial t} = \frac{\partial^2 T}{\partial x^2} + \frac{1}{k_M} \frac{\partial k_M}{\partial x} \frac{\partial T}{\partial x} \quad (11)$$

where g_S is calculated with Eq. (1). Additionally, it is assumed $\rho_S = \rho_L$ and $\alpha_M = k_M / (\rho c_M)$ is thermal diffusivity in the mushy zone. In the semi-infinite domain, the boundary conditions for temperature are given in Tab. 1.

Table 1. T_C is temperature of the cold wall, T_I is initial temperature, x_S is the position of the solidus line and x_L is the position of the liquidus line, $Q_{liq} = (T_{liq} - T_{sol}) / (T_F - T_{sol})$

x [m]	0	x_S	x_L	∞
T [K]	T_C	T_{sol}	T_{liq}	T_I
η [-]	0	η_S	η_L	∞
θ [-]	$\theta_S = 0$	$\theta_S = 1, \theta_M = 1$	$\theta_M = \theta_{liq}, \theta_L = 1$	$\theta_L = 0$

The conditions for jumps of heat fluxes at solid/mushy ($x = x_S$) and mushy/liquid ($x = x_L$) interfaces read

$$\text{at } x = x_S : k_S \frac{\partial T_S}{\partial x} - k_M \frac{\partial T_M}{\partial x} = (1 - g_{S,sol}) \rho L_{ht} \frac{dx_S}{dt} \quad (12)$$

$$\text{at } x = x_L : k_M \frac{\partial T_M}{\partial x} - k_L \frac{\partial T_L}{\partial x} = g_{S,liq} \rho L_{ht} \frac{dx_L}{dt} \quad (13)$$

where $g_{S,sol}$ and $g_{S,liq}$ are solid fractions calculated for the temperatures T_{sol} and T_{liq} using Eq. (1). To re-scale Eq. (11) non-dimensional temperatures $0 \leq \theta_k \leq 1$, where $k = S, M, L$ are introduced, in a solid, a mushy zone and a liquid

$$\theta_S = \frac{T - T_C}{T_{sol} - T_C}, \quad \theta_M = \frac{T - T_{sol}}{T_F - T_{sol}}, \quad \theta_L = \frac{T - T_I}{T_{liq} - T_I} \quad (14)$$

Next, the partial differential Eq. (11) is reduced to an ordinary differential equation, using the similarity variable $\eta = xg(t)$, $g(t) = 1/(2\sqrt{\alpha_S t})$; the boundary conditions for non-dimensional temperatures Q are given in Tab. 1. The variable transformation (see Appendix A) allows us to write Eq. (11) in the mushy zone ($\eta_S \leq \eta \leq \eta_L$) as

$$2\eta \frac{\alpha_S}{\alpha'_S} \frac{d\theta_M}{d\eta} + \frac{d^2\theta_M}{d\eta^2} + \frac{1}{k_M} \frac{dk_M}{d\eta} \frac{d\theta_M}{d\eta} = 0 \quad (15)$$

where

$$\frac{\alpha_S}{\alpha'_S} = \frac{c_M - L_{ht} \frac{dg_S}{dT}}{c_S \frac{k_M}{k_S}} \quad (16)$$

Since the volume fractions $g_S = 1$ in the solid ($0 \leq \eta \leq \eta_S$) and $g_L = 1$ in the liquid ($\eta_L \leq \eta \leq \infty$) are constant, we have $dg_S/dT = 0$ and $\alpha_S/\alpha'_S = 1$ in the solid phase and $dg_L/dT = 0$ and $\alpha_S/\alpha'_S = \alpha_S/\alpha'_L$ in the liquid phase. Therefore, the heat diffusion equations in the solid and liquid can be written as

$$2\eta \frac{d\theta_S}{d\eta} + \frac{d^2\theta_S}{d\eta^2} = 0 \quad : \quad 0 \leq \eta \leq \eta_S \quad (17)$$

$$2\eta \frac{\alpha_S}{\alpha'_L} \frac{d\theta_L}{d\eta} + \frac{d^2\theta_L}{d\eta^2} = 0 \quad : \quad \eta_L \leq \eta \leq \infty \quad (18)$$

respectively. As Eqs. (17) and (18) are linear ODE's their direct analytical solution is possible. Because in the mushy zone dg_S/dT , α_M , k_M are dependent on temperature, in order to obtain a linear form of Eq. (15), the averaging of the solid fraction derivative dg_S/dT in Eq. (16) is introduced

$$\left\langle \frac{dg_S}{dT} \right\rangle = \frac{1}{\Delta T} \int_{T_{sol}}^{T_{liq}} \frac{dg_S}{dT} dT, \quad \Delta T = T_{liq} - T_{sol} \quad (19)$$

Assuming that the averaged derivative of solid fraction (Eq. (19)) is equal to that resulting from the micro-segregation model (Eq. (1) or Eq. (2)) for an equivalent temperature T_{eq} (assumed to be constant over the range $\langle T_{sol}, T_{liq} \rangle$) one obtains condition used for the calculation of equivalent temperature T_{eq} in the mushy zone

$$\left\langle \frac{dg_S}{dT} \right\rangle = \frac{dg_S}{dT} \quad (20)$$

When the solid fraction g_S is calculated from the lever rule, see Eq. (1), the equivalent temperature reads

$$T_{eq} = T_F - \sqrt{(T_{liq} - T_F)(T_{sol} - T_F)} \quad (21)$$

if the Scheil model defined by Eq. (2) is used for g_S calculation, one obtains

$$T_{eq} = T_F - [(1 - k_P)A]^{-\frac{1-k_P}{2-k_P}} \quad (22)$$

$$A = \frac{1}{T_{liq} - T_{sol}} \left[(T_F - T_{liq})^{-\frac{1}{1-k_P}} - (T_F - T_{sol})^{-\frac{1}{1-k_P}} \right]$$

T_{eq} calculated with Eq. (21) or Eq. (22) is now used to determine the equivalent solid fraction $g_{S,eq} = \text{const}$ and material properties $k_{M,eq} = \text{const}$, $c_{M,eq} = \text{const}$ representative for the whole mushy zone. One notices when the thermal conductivity $k_M = k_{M,eq}$ is constant, the assumption $dk_M/d\eta = 0$ used by Chakaraborty and Dutta (2002) to derive Eq. (15) is justified. The averaging introduced in Eq. (19) and the employment

of the boundary conditions allow for the analytical integration of Eqs. (15)–(18) with $dk_M/d\eta = 0$ in the mushy zone, in the solid and in the liquid separately. The result are temperature profiles given by

$$\theta_S = \frac{\text{erf}(\eta)}{\text{erf}(\eta_S)} : 0 \leq \eta \leq \eta_S \quad (23)$$

$$\theta_M = \theta_{liq} \frac{\text{erf}(\sqrt{a}\eta) - \text{erf}(\sqrt{a}\eta_S)}{\text{erf}(\sqrt{a}\eta_L) - \text{erf}(\sqrt{a}\eta_S)} : \eta_S \leq \eta \leq \eta_L \quad (24)$$

$$\theta_L = \frac{\text{erfc}(\sqrt{b}\eta)}{\text{erfc}(\sqrt{b}\eta_L)} : \eta_L \leq \eta \leq \infty \quad (25)$$

where $b = c_S k_L / c_L k_S$ and

$$a = \frac{\alpha_S}{\alpha'_S} = \frac{c_{M,eq} - L_{ht} \left\langle \frac{dgs}{dT} \right\rangle}{c_S \frac{k_{M,eq}}{k_S}} \quad (26)$$

is the averaged coefficient, see Eqs. (15)–(16). Finally, the unknown positions of the solidus η_S and liquidus η_L lines are determined from the solution of the equation system obtained after substitution of Eqs. (23)–(25) into the boundary conditions for the jumps of heat fluxes obtained using Eqs. (12)–(14)

$$\theta_E \frac{d\theta_S}{d\eta} - r_{MS} \frac{d\theta_M}{d\eta} = \frac{2\eta_S(1 - g_{S,sol})}{St} \quad (27)$$

$$r_{MS} \frac{d\theta_M}{d\eta} - \theta_I r_{LS} \frac{d\theta_L}{d\eta} = \frac{2\eta_L g_{S,liq}}{St} \quad (28)$$

where $\theta_E = (T_{sol} - T_C) / (T_F - T_{sol})$, $r_{MS} = k_{M,eq} / k_S$, $\theta_I = (T_{liq} - T_1) / (T_F - T_{sol})$, $r_{LS} = k_L / k_S$, $St = c_S (T_F - T_{sol}) / L_{ht}$ are given constants. In Appendix B the derivation of jump conditions given by Eqs. (27)–(28) can be found.

3.1. Modification of the semi-analytical solution

Since Eq. (5) is solved in the given flow solver, the influence of the term containing the gradient of k_M on the solidification process is always present. Therefore, a direct comparison between the semi-analytical solution introduced by Chakaraborty and Dutta (2002) and the numerical solution to Eq. (5) is not possible when $k_S \neq k_L$.

To generalize the solution to Eq. (15), we introduce a number of intervals $N > 1$ in which T_{eq}^k is determined, $k = 1, \dots, N$; the complete description of the solution procedure for N intervals can be found in Appendix D. In the following, the case of two temperature intervals $N = 2$ is discussed as it is sufficient to present the main assumptions and problems of the modified semi-analytical solution.

In the case of two intervals: $\langle T_{sol}, T_1 \rangle$, $\langle T_1, T_{liq} \rangle$ the averaging introduced by Eq. (19) can be carried out in each interval separately

$$\left\langle \frac{dgs}{dT} \right\rangle \Big|_1 = \frac{1}{\Delta T_1} \int_{T_{sol}}^{T_1} \frac{dgs}{dT} dT, \quad \Delta T_1 = T_1 - T_{sol} \quad (29)$$

$$\left\langle \frac{dgs}{dT} \right\rangle \Big|_2 = \frac{1}{\Delta T_2} \int_{T_1}^{T_{liq}} \frac{dgs}{dT} dT, \quad \Delta T_2 = T_{liq} - T_1 \quad (30)$$

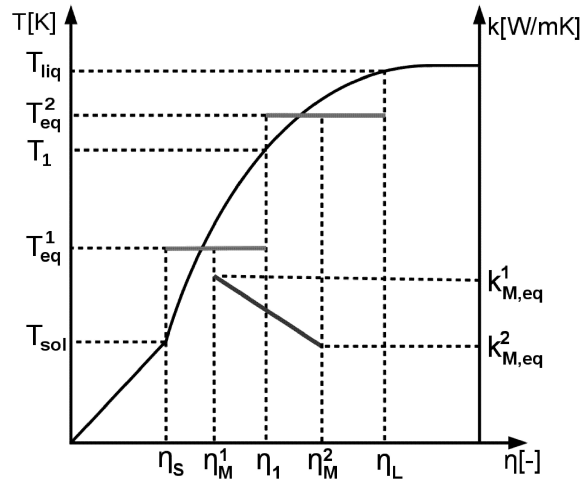


Fig. 2. A sketch of the modification to the semi-analytical solution, in this figure $k_S > k_L$ and $N = 2$

where T_1 is the unknown temperature inside the mushy zone as shown in Fig. 2. Next Eq. (20) must be solved in the two temperature intervals allowing the calculation of the equivalent temperatures

$$T_{eq}^1 = T_F - \sqrt{(T_{liq} - T_F)/A_1} \quad (31)$$

$$T_{eq}^2 = T_F - \sqrt{(T_{liq} - T_F)(T_1 - T_F)} \quad (32)$$

where

$$A_1 = \frac{1}{T_{liq} - T_1} \left[\frac{T_1 - T_{liq}}{T_1 - T_F} - \frac{T_{sol} - T_{liq}}{T_{sol} - T_F} \right] \quad (33)$$

for more details see Appendix C. Using the equivalent temperatures T_{eq}^1 and T_{eq}^2 constant in each interval, we calculate the solid volume fractions $g_{S,eq}^1$ and $g_{S,eq}^2$ and material properties for each temperature interval inside the mushy zone, e.g. $k_{M,eq}^1$, $k_{M,eq}^2$ as is shown in Fig. 2. Here we note that now the $k_{M,eq}^k$ distribution inside the mushy zone is piecewise constant. Thus, the last term on the RHS of Eq. (15) can be approximated by forward or backward differences (central differences are used when $N > 3$ as is shown in Appendix D), so that

$$b_1 = \frac{1}{k_{M,eq}^1} \frac{dk_M^1}{d\eta} \Big|_1 \approx \frac{1}{k_{M,eq}^1} \frac{k_{M,eq}^1 - k_{M,eq}^2}{\eta_M^1 - \eta_M^2} = \frac{k_S - k_L}{k_{M,eq}^1} \frac{g_{S,eq}^2 - g_{S,eq}^1}{\eta_M^2 - \eta_M^1} \quad (34)$$

$$b_2 = \frac{1}{k_{M,eq}^2} \frac{dk_M^2}{d\eta} \Big|_2 \approx \frac{1}{k_{M,eq}^2} \frac{k_{M,eq}^2 - k_{M,eq}^1}{\eta_M^2 - \eta_M^1} = \frac{k_S - k_L}{k_{M,eq}^2} \frac{g_{S,eq}^2 - g_{S,eq}^1}{\eta_M^2 - \eta_M^1} \quad (35)$$

where $\eta_M^1 = (\eta_S + \eta_1)/2$, $\eta_M^2 = (\eta_1 + \eta_L)/2$. The above approximation corresponds to the assumption of a constant thermal conductivity gradient $dk_M/dx = dk_M/d\eta g(t) = \text{const}$. Thus, a constant distribution of $k_{M,eq}$ in each temperature interval allows the introduction of a piecewise linear variation of the thermal conductivity coefficient k_M in the mushy zone. Using the latter assumption, Eq. (15) can be rewritten as

$$(2\eta a_1 + b_1) \frac{d\theta_M^1}{d\eta} + \frac{d^2\theta_M^1}{d\eta^2} = 0 \quad : \quad \eta_S \leq \eta \leq \eta_1 \quad (36)$$

$$(2\eta a_2 + b_2) \frac{d\theta_M^2}{d\eta} + \frac{d^2\theta_M^2}{d\eta^2} = 0 \quad : \quad \eta_1 \leq \eta \leq \eta_L \quad (37)$$

where $a_k, b_k, k = 1, 2$ are constants determined from Eq. (26) and Eqs. (34)–(35), respectively. Analytical solutions to Eqs. (36)–(37) read

$$\theta_M^1 = \theta_{liq}^1 \frac{\text{erf}[d_1(\eta)] - \text{erf}[d_1(\eta_S)]}{\text{erf}[d_1(\eta_1)] - \text{erf}[d_1(\eta_S)]} \quad (38)$$

$$\theta_M^2 = \theta_{liq}^2 \frac{\text{erf}[d_2(\eta)] - \text{erf}[d_2(\eta_1)]}{\text{erf}[d_2(\eta_L)] - \text{erf}[d_2(\eta_1)]} \quad (39)$$

where

$$d_k(\eta) = \sqrt{a_k} \eta + \frac{b_k}{2\sqrt{a_k}}, \quad k = 1, 2 \quad (40)$$

and $\theta_M^1 = (T - T_{sol})/(T_F - T_{sol})$, $\theta_{liq}^1 = (T_1 - T_{sol})/(T_F - T_{sol})$, $\theta_M^2 = (T - T_1)/(T_F - T_1)$, $\theta_{liq}^2 = (T_{liq} - T_1)/(T_F - T_1)$. We note, the second term in Eq. (40) is inherited from the finite difference approximation of the thermal conductivity gradient.

The remaining problem is how to determine the four unknowns depicted in Fig. 2: η_S, η_L, η_1 and temperature in the mushy zone T_1 . An equation required to determine T_1 is obtained from the condition of energy flux continuity inside the mushy zone (see Eq. (B5) in Appendix B). Hence, the boundary conditions for the heat fluxes at η_S, η_1 and η_L become

$$\theta_E \frac{d\theta_S}{d\eta} - r_{MS}^1 \frac{d\theta_M^1}{d\eta} = \frac{2\eta_S(1 - g_{S,sol})}{St_0} \quad (41)$$

$$\theta_{sol}^1 \frac{d\theta_M^1}{d\eta} - \frac{d\theta_M^2}{d\eta} = 0 \quad (42)$$

$$r_{MS}^2 \frac{d\theta_M^2}{d\eta} - \theta_{lRS} \frac{d\theta_L}{d\eta} = \frac{2\eta_L g_{S,liq}}{St_1} \quad (43)$$

where $r_{MS}^1 = k_{M,eq}^1/k_S$, $r_{MS}^2 = k_{M,eq}^2/k_S$, $\theta_{sol}^1 = (T_F - T_{sol})/(T_F - T_1)$, $St_0 = c_S(T_F - T_{sol})/L_{ht}$ and $St_1 = c_S(T_F - T_1)/L_{ht}$; the derivation of Eqs. (41)–(43) is given in Appendix B. Additionally, we note since the set of Eqs. (41)–(43) is non-linear, η_1 may be replaced by a linear combination of η_S and η_L . Hence, for the two temperature intervals $\eta_1 = (\eta_S + \eta_L)/2$ and thus all four unknowns can be determined.

As in the original solution, the analytically obtained temperature profiles given by Eqs. (23), (25), (38), (39) are used to build a non-linear set of equations after substitution into the boundary conditions given by Eqs. (41)–(43) as is shown in Appendix D. The obtained set of equations is solved using the Matlab *fsolve* non-linear equation solver, which uses either the Trust-Region Dogleg or Newton-Rhaphson method. We found that the results, i.e. values of η_S, T_1 and η_L do not depend on the solver used to obtain the solution. When $N = 2$, the initial value of the temperature inside the mushy zone T_1^I is set to $T_1^I = (T_{liq} + T_{sol})/2$. When $N \geq 3$ the initial values of the temperatures in the mushy zone sub-division points T_1^I where $l = 2, \dots, N-1$ are determined from the temperature profiles obtained in the previous iteration. The determination of subsequent T_1^I values is crucial for the convergence of the solution procedure with an increasing number of intervals.

The above semi-analytical solution is generalized with respect to the number of sub-domains $N \leq 8$ and its convergence is investigated. In Fig. 3a, the decreasing distances between the positions of the solidus η_S and liquidus lines η_L obtained with successively increasing numbers of temperature intervals N are depicted. Using solutions of successively refined temperature intervals, we are able to determine an interval number N independent solution with the aid of Richardson extrapolation (Schäfer, 2006). A comparison with a numerical solution obtained using the Star-CD solver is shown in Fig. 3b.

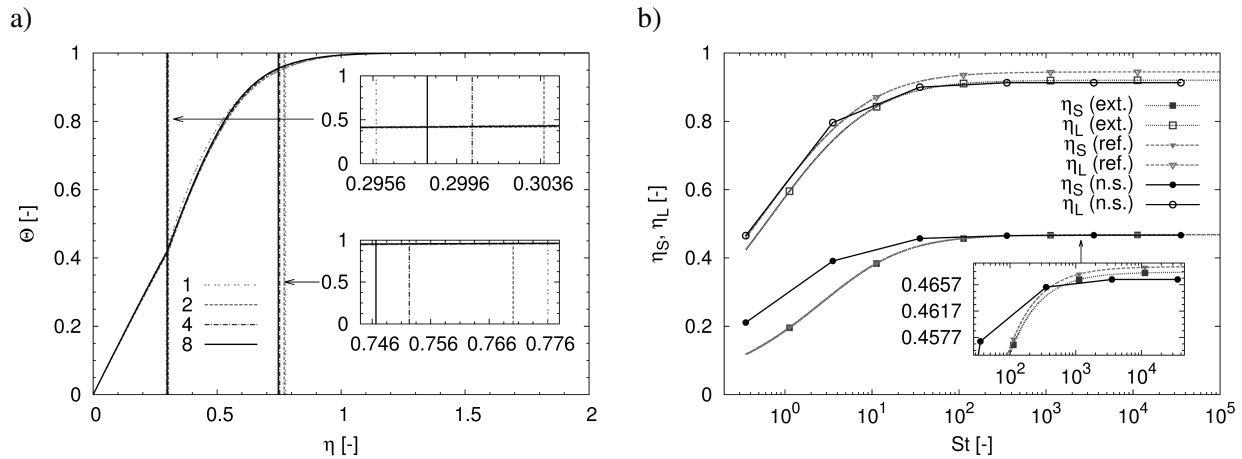


Fig. 3. a) Temperature profiles obtained with different numbers of averaging intervals $N = 1, 2, 4, 8$. b) A comparison of the semi-analytical solution with $N = 1$ (ref.), modified and interval number N independent semi-analytical solution (ext.) and numerical solution from the Star-CD code (n.s.)

3.2. Verification of the numerical model with the semi-analytical solution

The solidification algorithm was initially verified using material parameters from Voller and Brent (1989) for an aqueous solution of ammonium chloride NH_4 70% H_2O (see Tab. 2) and boundary conditions for temperature at $\eta = 0, T_C = 220$ K and $\eta \rightarrow \infty, T_C = 310$ K as in work of Chakaraborty and Dutta (2002). The similarity solutions presented in Figs 3, 4 are determined at time $t = 5000$ s.

Table 2. The material properties of an aqueous solution of ammonium chloride NH_4 70% H_2O

c [J/(kgK)]	ρ [kg/m ³]	k_S [W/(mK)]	k_L [W/(mK)]	L_{ht} [J/kg]	T_F [K]	T_{sol} [K]	T_{liq} [K]
3000	1078	0.4	0.1	3.18×10^5	633.59	257.95	305.95

Because of the disagreement between semi-analytical and numerical solutions obtained for this set of thermophysical parameters, we studied the influence of L_{ht} magnitude on the positions of the solidus and liquidus lines, emphasizing that L_{ht} is a continuous parameter in Eq. (26). This study allows us to find a range of Stefan numbers $St = c_s(T_F - T_{sol})/L_{ht}$, where the original semi-analytical solution ($k_S = k_L = k_M$) and its extension ($k_S \neq k_L \neq k_M$) can be used in the verification procedure. The range of the applicability of the semi-analytical solution was not discussed by Chakaraborty and Dutta (2002). In Fig. 3b we observe that when $L_{ht} \leq 1.12 \times 10^4$ J/kg, which corresponds to a Stefan number $St \geq 100$, the agreement between the interval number independent, semi-analytical solution and the numerical solution is satisfactory. Moreover, the difference between η_S, η_L positions predicted by the flow solver and the modified semi-analytical solution is smaller than the difference between the original solution and the present numerical results. This confirms the need to take into account the variation of the thermal conductivity coefficient k_M in the semi-analytical solution of Eq. (11).

When larger values of $L_{ht} \geq 1.12 \times 10^4$ J/kg are used, resulting in $St \leq 100$, the positions of the solidus line η_S predicted by the original or modified semi-analytical solutions and the numerical simulation disagree. The coincident shift of the solidus and liquidus lines towards the cold wall can be explained by the retardation of the solidification process caused by the rejection of a larger amount of the latent heat, see Fig. 3b. However, in the case of semi-analytical solutions, e.g. for $L_{ht} \leq 3.18 \times 10^5$ J/kg corresponding to $St \approx 3.5$, the change of the solidus line position is too rapid. In the forthcoming section we will show how the removal of the non-linearity from Eq. (12) affects the η_S, η_L positions.

3.3. Influence of non-linearity in the heat diffusion equation on mushy zone thickness

To assess the influence of the nonlinear term α_S/α'_S in Eq. (15) on the shift of the solidus line for $L_{ht} \geq 1.12 \times 10^4$ J/kg, $St \leq 100$, we rewrite Eq. (15) as a set of two ordinary differential equations that can be solved as an initial value problem

$$\frac{dT}{d\eta} = \varphi \tag{44}$$

$$\frac{d\varphi}{d\eta} = -\frac{2\eta\alpha_S}{\alpha'_S(T)}\varphi \tag{45}$$

where the coefficient α_S/α'_S is calculated directly with Eq. (16). The boundary conditions for the set of Eqs. (44)–(45) are given by $T = T_C$ for $\eta = 0$ and $T = T_I$ for $\eta \rightarrow \infty$. The latter boundary condition is obtained iteratively, because for the solution of the initial value problem both the temperature and the temperature gradient are required at $\eta = 0$. To remove effects associated with jumps of heat fluxes at the solidus and liquidus fronts (i.e. possible discontinuity in a temperature gradient profile, see Eqs. (12)–(13)) and disregard the influence of the term $\partial k/\partial x$ in this test case, we set the thermal conductivity coefficient to the constant value $k_M = k_S = k_L = 0.4$ Wm⁻²K⁻¹ in the whole domain $0 \leq \eta \leq 8$.

The comparison of results obtained from the original semi-analytical solution $N = 1$, the numerical solutions of the initial value problem in Matlab and the solution of the general energy conservation Eq. (5) in Star-CD is depicted in Fig. 4. In Fig. 4a, where $L_{ht} = 3.18 \times 10^3$ J/kg and $St \approx 309$, we can observe good agreement between both numerical solutions and the original semi-analytical solution. The main observation in Figure 4b is the disagreement of the semi-analytical solution and both numerical solutions when $L_{ht} = 3.18 \times 10^5$ J/kg and $St \approx 3.5$. This latter result coincides with results presented in Figure 3b. The second observation to be made from Fig. 4 is good agreement between both numerical solutions independently on the L_{ht} magnitude. These two observations confirm the influence of the linearization introduced to the semi-analytical solution of Eq. (15) on the artificial shift of the solidus line η_S , and thus explain the incorrect prediction of the mushy zone thickness and solidification fronts positions when $St \leq 100$.

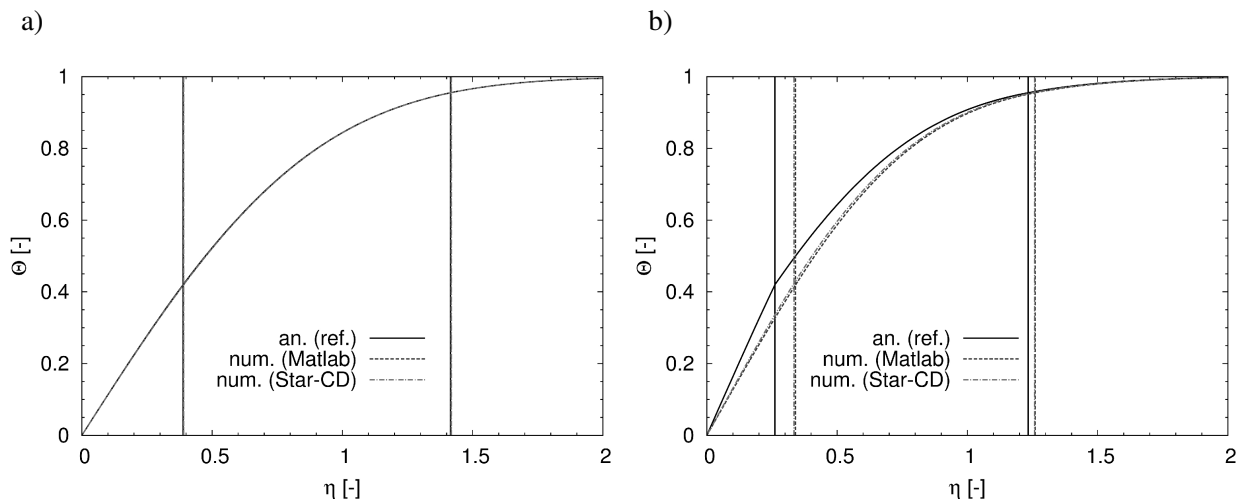


Fig. 4. Influence of the temperature averaging on the positions of solidus η_S and liquidus η_L lines. The semi-analytical solution $N = 1$ (solid line, ref.) is compared with numerical solution Matlab (dashed line) and solution of Eq. (5) from Star-CD (double-dotted line) obtained for $L_{ht} = 3.18 \times 10^3$ J/kg, $St \approx 309$ (left), $L_{ht} = 3.18 \times 10^5$ J/kg, $St \approx 3.5$ (right)

4. CONCLUSIONS

In this paper, a verification study of the binary-fluid solidification model coupled with the finite volume flow solver Star-CD is presented. We extend the semi-analytical solution to the 1D heat diffusion equation taking into account variable heat conduction coefficient inside the mushy zone. Afterwards, the range of applicability of this semi-analytical solution is analyzed demonstrating it can be used for verification of the numerical model of binary fluid solidification only when $St > 100$. For smaller Stefan numbers the non-linear effects related to the latent heat rejection become dominant. Hence, the linearization introduced to integrate the heat diffusion equation is not a sufficient approximation of the binary-fluid solidification process for large latent heat magnitudes.

This work was funded by the German Research Foundation (DFG) in the framework of the project “Multi-phase-based modeling, simulation and experimental validation of mold filling and solidification of metallic melts in the light of foreign particles and porosity.” SCHA: 814/132, AOBJ: 577070. We are also grateful to Prof. M. Peric and Dr. Huang Jianbo from CD-Adapco for discussions and technical support.

SYMBOLS

c	specific heat, $\text{Jkg}^{-1}\text{K}^{-1}$
f	mass fraction
g	volume fraction
g_i	i -th gravitational acceleration component, ms^{-2}
h	mixture enthalpy, Jkg^{-1}
k	thermal conductivity, $\text{Wm}^{-1}\text{K}^{-1}$
k_p	partition coefficient
m	total mass, kg
m_L	slope of liquidus line, $\text{K}\%^{-1}$
p	pressure, Nm^{-2}
q	heat flux, Wm^{-2}
t	time moment, s
u_i	i -th velocity component, ms^{-1}
x	spatial coordinate, m
x_S	position of the solidus line, m
x_L	position of the liquidus line, m
A	auxiliary constant
B	solvent concentration, m
C	solute concentration, %
D	diffusion coefficient, m^2s^{-1}
K	permeability coefficient, m^2
K_0	relative permeability coefficient, m^2
L	horizontal dimension of the computational domain, m
L_{ht}	latent heat of fusion, Jkg^{-1}
N	number of temperature intervals
N_c	number of CV's
T	temperature, K
V	volume of representative control volume, m^3
St	Stefan number

Greek symbols

α	thermal diffusivity, m^2s^{-1}
η	similarity variable
θ	non-dimensional temperature
λ	secondary dendrite arm spacing, m^2
μ_L	liquid alloy dynamic viscosity, $\text{kg m}^{-1}\text{s}^{-1}$
ρ	mixture density, kgm^{-3}
χ	thermal expansion coefficient, K^{-1}
ψ	solutal expansion coefficient

Subscripts/Superscripts

C	cold wall
E	eutectic
F	fusion
I	initial
L	liquid
M	mixture
S	solid
eq	equivalent
liq	liquidus
sol	solidus

Abbreviations

ODE ordinary differential equation

REFERENCES

- Banaszek J, Sereżyński M., 2012. The accuracy of a solid packing fraction model in recognizing zones of different dendritic structures. *Int. J. Heat Mass Transf.*, 55, 4334–4339. DOI: 10.1016/j.ijheatmasstransfer.2012.03.082.
- Bars L.M., Worster M.G., 2006. Interfacial conditions between pure fluid and a porous medium, implications for binary alloy solidification. *J. Fluid Mech.*, 550, 149–173. DOI: 10.1017/S0022112005007998.
- Bennon W.D., Incropera F.P., 1987. A continuum model for momentum, heat and species transport in binary solid-liquid phase change systems – I. Model formulation. *Int. J. Heat Mass Transf.*, 30, 2161–2170. DOI: 10.1016/0017-9310(87)90094-9.
- Bennon W.D., Incropera F.P., 1987. A continuum model for momentum, heat and species transport in binary solid-liquid phase change systems – II. Application to solidification in rectangular cavity. *Int. J. Heat Mass Transf.*, 30, 2161–2170. DOI: 10.1016/0017-9310(87)90095-0.
- Braga S.L., Viskanta R., 1990. Solidification of a binary solution on a cold isothermal surface, *Int. J. Heat Mass Transf.*, 33, 745–754. DOI: 10.1016/0017-9310(90)90172-Q.
- Chakarabarty S., Dutta P., 2002. An analytical solution for conduction dominated unidirectional solidification of binary mixtures. *Appl. Math. Model.*, 26, 545–561. DOI: 10.1016/S0307-904X(01)00073-7.
- Jakumeit J., Jana S., Waclawczyk T., Mehdizadeh A., Youani J., Buehrig-Polaczek A., 2012. Four-phase fully coupled mold-filling and solidification simulation for gas porosity prediction in aluminum sand casting. In *13th MCWASP*, Austria, June 17–22. DOI: 10.1088/1757-899X/33/1/012074.
- Kurz W., Fischer D.J., 1990. *Fundamentals of solidification*. Trans Tech Publications.
- Sereżyński M., Banaszek J., 2014. Front tracking approach to modeling binary alloy solidification: Accuracy verification and the role of dendrite growth kinetics. *Int. J. Num Meth. Heat Fluid Flow*, 24, 920–931. DOI: 10.1108/HFF-02-2013-0069.

- Voller V.R., Brent A.D., 1989. The modeling of heat, mass and solute transport in solidification systems. *Int. J. Heat Mass Transfer*, 32, 1719–1731. DOI: 10.1016/0017-9310(89)90054-9.
- Voller V.R., 1997. A similarity solution for the solidification of a multicomponent alloy. *Int. J. Heat Mass Transf.*, 40, 2869–2877. DOI: 10.1016/S0017-9310(96)00330-4.
- Waławczyk T., Sternel D., Schäfer M., 2011. Verification of binary fluid solidification model. In ICNAAM AIP Conference Proc., vol. 1389, Halkidiki, Greece. DOI: 10.1063/1.3636676.
- Waławczyk T., Schäfer M., 2016. Verification of binary fluid solidification model in the finite volume flow solver. *arXiv preprint arXiv:1507.01131*. Available at: <https://arxiv.org/ftp/arxiv/papers/1507/1507.01131.pdf>
- Wang Chao-Yang, Beckermann C., 1993. A two-phase mixture model of liquid-gas flow and heat transfer in capillary porous media – I. Formulation. *Int. J. Heat Mass Transf.*, 36, 2747–2758. DOI: 10.1016/0017-9310(93)90094-M.
- Wang Chao-Yang, Beckermann C., A two-phase mixture model of liquid-gas flow and heat transfer in capillary porous media – II. Application to pressure-driven boiling flow adjacent to a vertical heated plate. *Int. J. Heat Mass Transf.*, 36, 2759–2768. DOI: 10.1016/0017-9310(93)90095-N.
- Worster M.G., 1986. Solidification of an alloy from a cooled boundary. *J. Fluid Mech.*, 167, 481–501. DOI: 10.1017/S0022112086002938.

Received 20 July 2016

Received in revised form 26 January 2018

Accepted 05 February 2018

APPENDIX A

In this appendix, we describe the change of variables in Eq. (11) inside the mushy zone. The non-dimensional temperature θ in the solid, the mushy zone and the liquid is given by Eqs. (14). After substitution into Eq. (11) we obtain

$$\left(\frac{1}{\alpha_M} - \frac{\rho L_{ht}}{k_M} \frac{\partial g_S}{\partial T} \right) \frac{\partial \theta_M}{\partial t} = \frac{\partial^2 \theta_M}{\partial x^2} + \frac{1}{k_M} \frac{\partial k_M}{\partial x} \frac{\partial \theta_M}{\partial x} \quad (\text{A1})$$

The similarity variable $\eta = xg(t)$, $g(t) = 1/(2\sqrt{\alpha_S t})$ is used to rewrite temporal and spatial derivatives in Eq. (A1) in the non-dimensional form. The time derivative in Eq. (A1) becomes

$$\frac{\partial \theta_M}{\partial t} = \frac{d\theta_M}{d\eta} \frac{\partial \eta}{\partial t} = -2\alpha_S \eta g^2 \frac{d\theta_M}{d\eta} \quad (\text{A2})$$

The first and second order spatial derivatives read

$$\frac{\partial \theta_M}{\partial x} = \frac{d\theta_M}{d\eta} \frac{\partial \eta}{\partial x} = \frac{d\theta_M}{d\eta} g \quad (\text{A3})$$

$$\frac{\partial}{\partial x} \left(\frac{\partial \theta_M}{\partial x} \right) = \frac{d}{d\eta} \left(\frac{d\theta_M}{d\eta} \frac{\partial \eta}{\partial x} \right) \frac{\partial \eta}{\partial x} = \frac{d^2 \theta_M}{d\eta^2} g^2 \quad (\text{A4})$$

The second term on the RHS in Eq. (A1) can be written as

$$\frac{1}{k_M} \frac{\partial k_M}{\partial x} \frac{\partial \theta_M}{\partial x} = \frac{1}{k_M} \frac{dk_M}{d\eta} \frac{d\theta_M}{d\eta} g^2 \quad (\text{A5})$$

Using Eqs. (A1)–(A5) and notation introduced in Eq. (16) we obtain Eq. (15).

APPENDIX B

Here, we derive the Stefan conditions at the solidus front $x = x_s$, inside the mushy zone at $x = x_l$, $l = 1, \dots, N-1$ and at the liquidus front $x = x_L$. Let us integrate Eq. (9) in the $N+1$ infinitesimal control volumes $\delta x_k = x_k^+ - x_k^- \rightarrow 0$ where $k = S, l, L$, respectively. Since the jumps of temperature $[T] = 0$ at x_S, x_l, x_L and the jumps of the solid fraction $[g_s] = 0$ at x_l and $[g_s] \neq 0$ at x_S, x_L ; integrated in $N+1$ control volumes Eq. (9) reads

$$\text{at } x = x_S : -\rho L_{ht} \frac{dx_S}{dt} \int_{x_S^-}^{x_S^+} \frac{\partial g_S}{\partial x} dx = \int_{x_S^-}^{x_S^+} \frac{\partial}{\partial x} \left(k \frac{\partial T}{\partial x} \right) dx \quad (B1)$$

$$\text{at } x = x_l : \int_{x_l^-}^{x_l^+} \frac{\partial}{\partial x} \left(k \frac{\partial T}{\partial x} \right) dx = 0 \quad (B2)$$

$$\text{at } x = x_L : -\rho L_{ht} \frac{dx_L}{dt} \int_{x_L^-}^{x_L^+} \frac{\partial g_S}{\partial x} dx = \int_{x_L^-}^{x_L^+} \frac{\partial}{\partial x} \left(k \frac{\partial T}{\partial x} \right) dx \quad (B3)$$

where we make an assumption $dx_k/dt = \text{const}$ in $\delta x_k \rightarrow 0$ for $k = S, L$. After spatial integration, taking into account the extraction of heat flux from the semi-infinite domain at $x = 0$ and orientation of normal vectors at the faces of the 1D control volumes δx_k , we obtain

$$\text{at } x = x_S : \rho L_{ht} \frac{dx_S}{dt} (1 - g_{S,sol}) = k_S \frac{\partial T_S}{\partial x} - k_M^l \frac{\partial T_M^l}{\partial x} \quad (B4)$$

$$\text{at } x = x_l : \frac{\partial T_M^l}{\partial x} - \frac{\partial T_M^{l+1}}{\partial x} = 0 \quad (B5)$$

$$\text{at } x = x_L : \rho L_{ht} \frac{dx_L}{dt} g_{S,liq} = k_M^{l+1} \frac{\partial T_M^{l+1}}{\partial x} - k_L \frac{\partial T_L}{\partial x} \quad (B6)$$

where $g_{S,sol} = g_S(T_{sol})$, $g_{S,liq} = g_S(T_{liq})$ and $l = 1, \dots, N-1$. Next, we show how non-dimensional temperatures θ and similarity variable η are introduced into Eqs. (B4)–(B6). Let us first note that the velocities of the solidification fronts may be rewritten as

$$\text{at } x = x_S : \frac{dx_S}{dt} = \frac{1}{g} \frac{\partial \eta_S}{\partial t} - \frac{\eta_S}{g^2} \frac{\partial g}{\partial t} = 2\alpha_S g \eta_S \quad (B7)$$

$$\text{at } x = x_L : \frac{dx_L}{dt} = \frac{1}{g} \frac{\partial \eta_L}{\partial t} - \frac{\eta_L}{g^2} \frac{\partial g}{\partial t} = 2\alpha_S g \eta_L \quad (B8)$$

since we are searching for a stationary solution to Eq. (11) at large times t . The non-dimensional temperatures in the solid, the mushy zone k -th interval and in the liquid read

$$\theta_S = \frac{T - T_C}{T_{sol} - T_C}, \quad \theta_M^k = \frac{T - T_{k-1}}{T_F - T_{k-1}}, \quad \theta_L = \frac{T - T_I}{T_{liq} - T_I} \quad (B9)$$

where $k = 1, \dots, N$ and where for $k = 1 : T_0 = T_{sol}$. Substitution of Eqs. (B7)–(B9) in Eqs. (B4)–(B6) results in

$$\theta_E \frac{d\theta_S}{d\eta} - r_{MS}^1 \frac{d\theta_M^1}{d\eta} = \frac{2\eta_S(1 - g_{S,sol})}{St_0} \quad (B10)$$

$$\theta_{sol}^l \frac{d\theta_M^l}{d\eta} - \frac{d\theta_M^{l+1}}{d\eta} = 0 \quad (B11)$$

$$r_{MS}^N \frac{d\theta_M^N}{d\eta} - \theta_I r_{LS} \frac{d\theta_L}{d\eta} = \frac{2\eta_L g_{S,liq}}{St_{N-1}} \quad (B12)$$

where $l = 1, \dots, N-1$, $r_{MS}^l = k_M^l/k_S$, $St_0 = c_S(T_F - T_{sol})/L_{ht}$, $\theta_{sol}^l = (T_F - T_{l-1})/(T_F - T_I)$ where for $l+1 = N : T_N = T_{liq}$, $\theta_I = (T_{liq} - T_I)/(T_F - T_{N-1})$, $St_{N-1} = c_S(T_F - T_{N-1})/L_{ht}$.

APPENDIX C

In this appendix, we show how to determine the equivalent temperatures T_{eq}^k inside the $k = 1, \dots, N$ intervals introduced in the mushy zone for averaging. The temperature averaged solid fraction gradient is calculated in the k -th temperature interval

$$\left\langle \frac{dg_S}{dT} \right\rangle_k = \frac{1}{\Delta T_k} \int_{T_{k-1}}^{T_k} \frac{dg_S}{dT} dT, \quad \Delta T_k = T_k - T_{k-1} \quad (C1)$$

where for $k = 1 : T_0 = T_{sol}$ and for $k = N : T_N = T_{liq}$. Since the temperature gradient of the solid fraction g_S defined in Eq. (1) reads

$$\frac{dg_S}{dT} = \frac{1}{1 - k_P} \left[\frac{1}{T - T_F} - \frac{T - T_{liq}}{(T - T_F)^2} \right] \quad (C2)$$

Eq. (C1) after integration becomes

$$\left\langle \frac{dg_S}{dT} \right\rangle_k = \frac{1}{(1 - k_P)\Delta T_k} \left(\frac{T_k - T_{liq}}{T_k - T_F} - \frac{T_{k-1} - T_{liq}}{T_{k-1} - T_F} \right), \quad \Delta T_k = T_k - T_{k-1} \quad (C3)$$

Since all temperatures in Eq. (C3) are known, the expression given by Eq. (C3) is constant in each interval k . Therefore, using approximation given by Eq. (20) and Eq. (C2), we write

$$A_k = (1 - k_P) \left\langle \frac{dg_S}{dT} \right\rangle_k = \left[\frac{1}{T_{eq}^k - T_F} - \frac{T_{eq}^k - T_{liq}}{(T_{eq}^k - T_F)^2} \right] \quad (C4)$$

Finally, from Eq. (C4) the equivalent temperature inside the k -th temperature interval reads

$$T_{eq}^k = T_F - \sqrt{\frac{T_{liq} - T_F}{A_k}} \quad (C5)$$

One notices that when $k = N$ and $T_N = T_{liq}$ then $A_N = 1/(T_{N-1} - T_F)$ and

$$T_{eq}^N = T_F - \sqrt{(T_{liq} - T_F)(T_{N-1} - T_F)} \quad (C6)$$

in particular for $N = 1$ Eq. (21) is recovered. One notices, $A_k < 0$ as $T_{eq}^k < T_F$ and $T_{eq}^k < T_{liq}$, thus the temperature product under square root in Eq. (C5) or (C6) and resulting T_{eq}^k are always positive.

APPENDIX D

Herein, the solution procedure for the set of $N + 1$ non-linear equations obtained from the conditions for heat fluxes in the mushy zone is described. This solution is required to find the unknowns $\eta_S, \dots, T_l, \dots, \eta_L$ where $l = 1, \dots, N-1$ denotes a number of unknown temperatures T_l at points

$$\eta_l = \eta_S + \frac{l}{N}(\eta_L - \eta_S) \quad (D1)$$

and $N \geq 2$ is the number of temperature intervals introduced for averaging. For simplicity, all following equations are derived using the lever rule model given by Eq. (1). First, we note the introduction of N averaging intervals $\Delta T_l = T_l - T_{sol}, \dots, \Delta T_k = T_k - T_{k-1}, \dots, \Delta T_N = T_{liq} - T_{N-1}$ where for $k = 1 : T_0 = T_{sol}$ and for $k = N : T_N = T_{liq}$ increases the number of the heat diffusion equations that must be solved to obtain piecewise temperature profiles. The set of $N+2$ ODE's that must be solved reads

$$2\eta \frac{d\theta_S}{d\eta} + \frac{d^2\theta_S}{d\eta^2} = 0, \quad 0 \leq \eta \leq \eta_S \quad (D2)$$

$$(2\eta a_k + b_k) \frac{d\theta_M^k}{d\eta} + \frac{d^2\theta_M^k}{d\eta^2} = 0, \quad \eta_{k-1} \leq \eta \leq \eta_k \quad (D3)$$

$$2\eta \frac{\alpha_S}{\alpha_L} \frac{d\theta_L}{d\eta} + \frac{d^2\theta_L}{d\eta^2} = 0, \quad \eta_L \leq \eta \leq \infty \quad (D4)$$

where for $k = 1 : \eta_0 = \eta_S$ and for $k = N : \eta_N = \eta_L$. Analytical solutions to Eqs. (D2)–(D4) are given by non-dimensional temperature profiles, written employing the notation introduced in Eq. (40)

$$\theta_S = \frac{\text{erf}(\eta)}{\text{erf}(\eta_S)} : 0 \leq \eta \leq \eta_S \quad (D5)$$

$$\theta_M^k = \theta_{liq}^k \frac{\text{erf}[d_k(\eta)] - \text{erf}[d_k(\eta_{k-1})]}{\text{erf}[d_k(\eta_k)] - \text{erf}[d_k(\eta_{k-1})]} : \eta_S \leq \eta \leq \eta_L \quad (D6)$$

$$\theta_L = \frac{\text{erfc}(\sqrt{b}\eta)}{\text{erfc}(\sqrt{b}\eta_L)} : \eta_L \leq \eta \leq \infty \quad (D7)$$

where $\theta_M^k, \theta_{liq}^k$ read

$$\theta_M^k = \frac{T - T_{k-1}}{T_F - T_{k-1}}, \quad \theta_{liq}^k = \frac{T_k - T_{k-1}}{T_F - T_{k-1}} \quad (D8)$$

The above formulation assures the continuity of temperature at points $\eta_S, \dots, \eta_l, \dots, \eta_L$, where $l = 1, \dots, N-1$ and $k = 1, \dots, N$.

In the second step, we determine constants a_k, b_k present in Eqs. (D6), see also Eq. (37). Knowing T_{eq}^k from Eq. (C5) for $k = 1, \dots, N$ allows the calculation of the representative solid fractions and material properties inside each of the k -th temperature intervals

$$g_S^k = \frac{1}{1 - k_P} \frac{T_{eq}^k - T_{liq}}{T_{eq}^k - T_F} \quad (D9)$$

$$c_M^k = g_S^k c_S + (1 - g_S^k) c_L \quad (D10)$$

$$k_M^k = g_S^k k_S + (1 - g_S^k) k_L \quad (D11)$$

and hence coefficients α_S/α'_S in Eq. (15) can be also determined

$$a_k = \frac{\alpha_S}{\alpha'_S} \Big|_k = \frac{c_M^k - L_{ht} \left\langle \frac{dgs}{dT} \right\rangle \Big|_k}{c_S \frac{k_M^k}{k_S}} \quad (D12)$$

The contribution from the thermal conductivity coefficient gradient b_k is approximated by central differences for $k = 2, \dots, N-1$.

$$b_k = \frac{1}{k_M} \frac{dk_M}{d\eta} \Big|_k \approx \frac{1}{k_M^k} \frac{k_M^{k+1} - k_M^{k-1}}{\eta_M^{k+1} - \eta_M^{k-1}} = \frac{k_S - k_L}{k_{M,eq}^k} \frac{g_{S,eq}^{k+1} - g_{S,eq}^{k-1}}{\eta_M^{k+1} - \eta_M^{k-1}} \quad (D13)$$

or forward and backward differences for $k = 1$ or $k = N$ respectively, see Eqs. (34)–(35). The unknown positions η_M^k are determined as a linear combination of η_S and η_L

$$\eta_M^k = \eta_{k-1} + \frac{1}{2}(\eta_k - \eta_{k-1}) \quad (D14)$$

where η_k is obtained from Eq. (D1).

In the third step we formulate a set of non-linear equations required to determine the unknowns $\eta_S, \dots, T_l, \dots, \eta_L$. After substitution of Eqs. (D5)–(D7) into the boundary conditions for heat fluxes given by Eqs. (B10)–(B12); the set of $N+1$ non-linear equations read

$$\frac{\theta_E \exp(-\eta_S^2)}{\operatorname{erf}(\eta_S)} - \frac{r_{MS}^1 \theta_{liq}^1 \sqrt{a_1} \exp(-d_1(\eta_S)^2)}{\operatorname{erf}(d_1(\eta_1)) - \operatorname{erf}(d_1(\eta_S))} = \frac{\sqrt{\pi} \eta_S (1 - g_{S,sol})}{St_0} \quad (D15)$$

$$\frac{\theta_{sol}^l \theta_{liq}^l \sqrt{a_l} \exp(-d_l(\eta_l)^2)}{\operatorname{erf}(d_l(\eta_l)) - \operatorname{erf}(d_l(\eta_{l-1}))} = \frac{\theta_{liq}^{l+1} \sqrt{a_{l+1}} \exp(-d_{l+1}(\eta_l)^2)}{\operatorname{erf}(d_{l+1}(\eta_{l+1})) - \operatorname{erf}(d_{l+1}(\eta_l))} \quad (D16)$$

$$\frac{r_{MS}^N \theta_{liq}^N \sqrt{a_N} \exp(-d_N(\eta_L)^2)}{\operatorname{erf}(d_N(\eta_L)) - \operatorname{erf}(d_N(\eta_{N-1}))} + \frac{\theta_l r_{LS} \sqrt{b} \exp(-b\eta_L^2)}{\operatorname{erfc}(\sqrt{b}\eta_L)} = \frac{\sqrt{\pi} \eta_L g_{S,liq}}{St_{N-1}} \quad (D17)$$

where $g_{S,sol}, g_{S,liq}$ are solid volume fractions obtained for the temperatures T_{sol} and T_{liq} , see Eq. (1). The solution of the set of Eqs. (D15)–(D17) using a non-linear equation solver allows to obtain the vector of $N+1$ unknowns $\eta_S, \dots, T_l, \dots, \eta_L$ where $l = 1, \dots, N-1$. After substitution of $\eta_S, \dots, T_l, \dots, \eta_L$ into the non-dimensional temperatures profiles given by Eqs. (D5)–(D7) the final solution is obtained.